

1 **MitoChime: A Machine-Learning Pipeline for**
2 **Detecting PCR-Induced Chimeras in**
3 **Mitochondrial Illumina Reads**

4 A Special Project Proposal
5 Presented to
6 the Faculty of the Division of Physical Sciences and Mathematics
7 College of Arts and Sciences
8 University of the Philippines Visayas
9 Miag-ao, Iloilo

10 In Partial Fulfillment
11 of the Requirements for the Degree of
12 Bachelor of Science in Computer Science

13 by

14 Duranne Duran
15 Yvonne Lin
16 Daniella Pailden

17 Adviser
18 Francis D. Dimzon, Ph.D.

19 December 5, 2025

Contents

21	1 Introduction	1
22	1.1 Overview	1
23	1.2 Problem Statement	3
24	1.3 Research Objectives	4
25	1.3.1 General Objective	4
26	1.3.2 Specific Objectives	4
27	1.4 Scope and Limitations of the Research	5
28	1.5 Significance of the Research	6
29	2 Review of Related Literature	7
30	2.1 The Mitochondrial Genome	7
31	2.1.1 Mitochondrial Genome Assembly	8

32	2.2 PCR Amplification and Chimera Formation	9
33	2.3 Existing Traditional Approaches for Chimera Detection	10
34	2.3.1 UCHIME	11
35	2.3.2 UCHIME2	12
36	2.3.3 CATch	13
37	2.3.4 ChimPipe	14
38	2.4 Machine Learning Approaches for Chimera and Sequence Quality	
39	Detection	15
40	2.4.1 Feature-Based Representations of Genomic Sequences . . .	16
41	2.5 Synthesis of Chimera Detection Approaches	18
42	3 Research Methodology	21
43	3.1 Research Activities	21
44	3.1.1 Data Collection	22
45	3.1.2 Feature Extraction Pipeline	26
46	3.1.3 Machine Learning Model Development	29
47	3.1.4 Model Benchmarking, Hyperparameter Optimization, and	
48	Evaluation	30
49	3.1.5 Feature Importance and Interpretation	31

50	3.1.6 Validation and Testing	32
51	3.1.7 Documentation	33
52	3.2 Calendar of Activities	34
53	4 Results and Discussion	35
54	4.1 Descriptive Analysis of Features	35
55	4.1.1 Univariate Distributions	36
56	4.2 Baseline Classification Performance	38
57	4.3 Effect of Hyperparameter Tuning	39
58	4.4 Detailed Evaluation of Representative Models	41
59	4.4.1 Confusion Matrices and Error Patterns	42
60	4.4.2 ROC and Precision–Recall Curves	43
61	4.5 Feature Importance and Biological Interpretation	45
62	4.5.1 Permutation Importance of Individual Features	45
63	4.5.2 Feature Family Importance	46
64	4.6 Summary of Findings	48

⁶⁵ List of Figures

⁶⁶	3.1 Process Diagram of Special Project	22
⁶⁷	4.1 Kernel density plots of six key features comparing clean and	
⁶⁸	chimeric reads.	37
⁶⁹	4.2 Test F1 of all baseline classifiers, showing that no single model	
⁷⁰	clearly dominates and several achieve comparable performance. . .	39
⁷¹	4.3 Comparison of test F1 (left) and ROC–AUC (right) for baseline and	
⁷²	tuned models. Hyperparameter tuning yields small but consistent	
⁷³	gains, particularly for tree-based ensembles.	41
⁷⁴	4.4 Confusion matrices for the four representative models on the held-	
⁷⁵	out test set. All models show more false negatives (chimeric reads	
⁷⁶	called clean) than false positives.	43
⁷⁷	4.5 ROC (left) and precision–recall (right) curves for the four represen-	
⁷⁸	tative models on the held-out test set. Tree-based ensembles cluster	
⁷⁹	closely, with logistic regression performing slightly but consistently	
⁸⁰	worse.	44

81	4.6 Permutation-based feature importance for four representative clas-	
82	sifiers. Clipping and k-mer composition features are generally the	
83	strongest predictors, whereas microhomology and other alignment	
84	metrics contribute minimally.	46
85	4.7 Aggregated feature family importance across four models. Clipping	
86	and k-mer compositional shifts are consistently the dominant con-	
87	tributors, while SA_structure, Micro_homology, and other features	
88	contribute minimally.	48

List of Tables

89	2.1 Comparison of Chimera Detection Methods	19
90	2.1 Comparison of Chimera Detection Methods	19
91	3.1 Timetable of Activities	34
92	3.1 Timetable of Activities	34
92	4.1 Performance of baseline classifiers on the held-out test set.	39
93	4.1 Performance of baseline classifiers on the held-out test set.	39
93	4.2 Performance of tuned classifiers on the held-out test set.	40
93	4.2 Performance of tuned classifiers on the held-out test set.	40

⁹⁴ **Chapter 1**

⁹⁵ **Introduction**

⁹⁶ **1.1 Overview**

⁹⁷ The rapid advancement of next-generation sequencing (NGS) technologies has
⁹⁸ transformed genomic research by enabling high-throughput and cost-effective
⁹⁹ DNA analysis (Metzker, 2010). Among current platforms, Illumina sequencing
¹⁰⁰ remains the most widely adopted, capable of producing millions of short reads
¹⁰¹ that can be assembled into reference genomes or analyzed for genetic variation
¹⁰² (Bentley et al., 2008; Glenn, 2011). Despite its high base-calling accuracy,
¹⁰³ Illumina sequencing is prone to artifacts introduced during library preparation,
¹⁰⁴ particularly polymerase chain reaction (PCR)-induced chimeras, which are ar-
¹⁰⁵ tificial hybrid sequences that do not exist in the true genome (Judo, Wedel, &
¹⁰⁶ Wilson, 1998).

¹⁰⁷ PCR chimeras form when incomplete extension products from one template

anneal to an unrelated DNA fragment and are extended, creating recombinant reads (Qiu et al., 2001). In mitochondrial genome assembly, such artifacts are especially problematic because the mitochondrial genome is small, circular, and often repetitive (Boore, 1999; Cameron, 2014). Even a small number of chimeric or misjoined reads can reduce assembly contiguity and introduce false junctions during organelle genome reconstruction (Dierckxsens, Mardulyn, & Smits, 2017; Hahn, Bachmann, & Chevreux, 2013; Jin et al., 2020). Existing assembly tools such as GetOrganelle and MITObim assume that input reads are largely free of such artifacts (Hahn et al., 2013; Jin et al., 2020). Consequently, undetected chimeras may produce fragmented assemblies or misidentified organellar boundaries. To ensure accurate reconstruction of mitochondrial genomes, a reliable method for detecting and filtering PCR-induced chimeras before assembly is essential.

This study focuses on mitochondrial sequencing data from the genus *Sardinella*, a group of small pelagic fishes widely distributed in Philippine waters. Among them, *Sardinella lemuru* (Bali sardinella) is one of the country's most abundant and economically important species, providing protein and livelihood to coastal communities (Labrador, Agmata, Palermo, Ravago-Gotanco, & Pante, 2021; Willette, Bognot, Mutia, & Santos, 2011). Accurate mitochondrial assemblies are critical for understanding its population genetics, stock structure, and evolutionary history. However, assembly pipelines often encounter errors or fail to complete due to undetected chimeric reads. To address this gap, this research introduces MitoChime, a machine learning pipeline designed to detect and filter PCR-induced chimeric reads using both alignment-based and sequence-derived statistical features. The tool aims to provide bioinformatics laboratories, partic-

₁₃₃ ularly the Philippine Genome Center Visayas (PGC Visayas), with an efficient
₁₃₄ solution for improving mitochondrial genome reconstruction.

₁₃₅ 1.2 Problem Statement

₁₃₆ While NGS technologies have revolutionized genomic data acquisition, the ac-
₁₃₇ curacy of mitochondrial genome assembly remains limited by artifacts produced
₁₃₈ during PCR amplification. These chimeric reads can distort assembly graphs and
₁₃₉ cause misassemblies, with particularly severe effects in small, circular mitochon-
₁₄₀ drial genomes (Boore, 1999; Cameron, 2014). Existing assembly pipelines such
₁₄₁ as GetOrganelle, MITObim, and NOVOPlasty assume that sequencing reads are
₁₄₂ free of such artifacts (Dierckxsens et al., 2017; Hahn et al., 2013; Jin et al., 2020).
₁₄₃ At PGC Visayas, several mitochondrial assemblies have failed or yielded incom-
₁₄₄ plete contigs despite sufficient coverage, suggesting that undetected chimeric reads
₁₄₅ compromise assembly reliability. Meanwhile, existing chimera detection tools such
₁₄₆ as UCHIME and VSEARCH were developed primarily for amplicon-based com-
₁₄₇ munity analysis and rely heavily on reference or taxonomic comparisons (Edgar,
₁₄₈ Haas, Clemente, Quince, & Knight, 2011; Rognes, Flouri, Nichols, Quince, &
₁₄₉ Mahé, 2016). These approaches are unsuitable for single-species organellar data,
₁₅₀ where complete reference genomes are often unavailable. Therefore, there is a
₁₅₁ pressing need for a reference-independent, data-driven tool capable of detecting
₁₅₂ and filtering PCR-induced chimeras in mitochondrial sequencing datasets.

₁₅₃ **1.3 Research Objectives**

₁₅₄ **1.3.1 General Objective**

₁₅₅ This study aims to develop and evaluate a machine learning-based pipeline (Mi-
₁₅₆ toChime) that detects PCR-induced chimeric reads in *Sardinella lemuru* mito-
₁₅₇ chondrial sequencing data in order to improve the quality and reliability of down-
₁₅₈ stream mitochondrial genome assemblies.

₁₅₉ **1.3.2 Specific Objectives**

₁₆₀ Specifically, the study aims to:

- ₁₆₁ 1. construct simulated *Sardinella lemuru* Illumina paired-end datasets contain-
₁₆₂ ing both clean and PCR-induced chimeric reads,
- ₁₆₃ 2. extract alignment-based and sequence-based features such as k-mer compo-
₁₆₄ sition, junction complexity, and split-alignment counts from both clean and
₁₆₅ chimeric reads,
- ₁₆₆ 3. train, validate, and compare supervised machine-learning models for classi-
₁₆₇ fying reads as clean or chimeric,
- ₁₆₈ 4. determine feature importance and identify indicators of PCR-induced
₁₆₉ chimerism,
- ₁₇₀ 5. integrate the optimized classifier into a modular and interpretable pipeline
₁₇₁ deployable on standard computing environments at PGC Visayas.

172 1.4 Scope and Limitations of the Research

173 This study focuses on detecting PCR-induced chimeric reads in Illumina paired-
174 end mitochondrial sequencing data from *Sardinella lemuru*. The decision to re-
175 strict the taxonomic scope to a single species is based on four considerations:
176 (1) to limit interspecific variation in mitochondrial genome size, GC content, and
177 repetitive regions so that differences in read patterns can be attributed more di-
178 rectly to PCR-induced chimerism; (2) to align the analysis with relevant *S. lemuru*
179 sequencing projects at PGC Visayas; (3) to take advantage of the availability of *S.*
180 *lemuru* mitochondrial assemblies and raw datasets in public repositories such as
181 the National Center for Biotechnology Information (NCBI), which facilitates refer-
182 ence selection and benchmarking; and (4) to develop a tool that directly supports
183 local studies on *S. lemuru* population structure and fisheries management.

184 The study emphasizes `wgsim`-based simulations and selected empirical mito-
185 chondrial datasets from *S. lemuru*. It excludes naturally occurring chimeras, nu-
186 clear mitochondrial pseudogenes (NUMTs), and large-scale assembly rearrange-
187 ments in nuclear genomes. Feature extraction is restricted to low-dimensional
188 alignment and sequence statistics, such as k-mer frequency profiles, GC content,
189 read length, soft and hard clipping metrics, split-alignment counts, and map-
190 ping quality, rather than high-dimensional deep learning embeddings. This de-
191 sign keeps model behaviour interpretable and ensures that the pipeline can be
192 run on standard workstations at PGC Visayas. Testing on long-read platforms
193 (e.g., Nanopore, PacBio) and other taxa is outside the scope of this project; the
194 implemented pipeline is evaluated only on short-read *S. lemuru* datasets.

¹⁹⁵ **1.5 Significance of the Research**

¹⁹⁶ This research provides both methodological and practical contributions to mi-
¹⁹⁷tochondrial genomics and bioinformatics. First, MitoChime filters PCR-induced
¹⁹⁸ chimeric reads prior to genome assembly, with the goal of improving the con-
¹⁹⁹tiguity and correctness of *Sardinella lemuru* mitochondrial assemblies. Second,
²⁰⁰ it replaces informal manual curation with a documented workflow, improving au-
²⁰¹tomation and reproducibility. Third, the pipeline is designed to run on computing
²⁰² infrastructures commonly available in regional laboratories, enabling routine use
²⁰³ at facilities such as PGC Visayas. Finally, more reliable mitochondrial assemblies
²⁰⁴ for *S. lemuru* provide a stronger basis for downstream applications in the field of
²⁰⁵ fisheries and genomics.

²⁰⁶ **Chapter 2**

²⁰⁷ **Review of Related Literature**

²⁰⁸ This chapter presents an overview of the literature relevant to the study. It
²⁰⁹ discusses the biological and computational foundations underlying mitochondrial
²¹⁰ genome analysis and assembly, as well as existing tools, algorithms, and techniques
²¹¹ related to chimera detection and genome quality assessment. The chapter aims to
²¹² highlight the strengths, limitations, and research gaps in current approaches that
²¹³ motivate the development of the present study.

²¹⁴ **2.1 The Mitochondrial Genome**

²¹⁵ Mitochondrial genome (mtDNA) is a small, typically circular molecule found in
²¹⁶ most eukaryotes. It encodes essential genes involved in oxidative phosphorylation
²¹⁷ and energy metabolism. Because of its conserved structure, mtDNA has become
²¹⁸ a valuable genetic marker for studies in population genetics and phylogenetics
²¹⁹ (Anderson et al., 1981; Boore, 1999). In animal species, the mitochondrial genome

220 ranges from 15–20 kilobase and contains 13 protein-coding genes, 22 tRNAs, and
221 two rRNAs arranged compactly without introns (Gray, 2012). In comparison to
222 nuclear DNA, the ratio of the number of copies of mtDNA is higher and has
223 simple organization which make it particularly suitable for genome sequencing
224 and assembly studies (Dierckxsens et al., 2017).

225 2.1.1 Mitochondrial Genome Assembly

226 Mitochondrial genome assembly refers to the reconstruction of the complete mito-
227 chondrial DNA (mtDNA) sequence from raw or fragmented sequencing reads. It is
228 conducted to obtain high-quality, continuous representations of the mitochondrial
229 genome that can be used for a wide range of analyses, including species identi-
230 fication, phylogenetic reconstruction, evolutionary studies, and investigations of
231 mitochondrial diseases. Because mtDNA evolves rapidly, its assembled sequence
232 provides valuable insights into population structure, lineage divergence, and adap-
233 tive evolution across taxa (Boore, 1999). Compared to nuclear genome assembly,
234 assembling the mitochondrial genome is often considered more straightforward but
235 still encounters technical challenges such as the formation of chimeric reads. Com-
236 monly used tools for mitogenome assembly such as GetOrganelle and MITObim
237 operate under the assumption of organelle genome circularity, and are vulnerable
238 when chimeric reads disrupt this circular structure, resulting in assembly errors
239 (Hahn et al., 2013; Jin et al., 2020).

240 2.2 PCR Amplification and Chimera Formation

241 PCR plays an important role in NGS library preparation, as it amplifies target
242 DNA fragments for downstream analysis. However as previously mentioned, the
243 amplification process can also introduce chimeric reads which compromises the
244 quality of the input reads supplied to sequencing or assembly workflows. Chimeras
245 typically arise when incomplete extension occurs during a PCR cycle. This causes
246 the DNA polymerase to switch from one template to another and generate hy-
247 brid recombinant molecules (Judo et al., 1998). Artificial chimeras are produced
248 through such amplification errors, whereas biological chimeras occur naturally
249 through genomic rearrangements or transcriptional events.

250 In the context of amplicon-based sequencing, the presence of chimeras can in-
251 flate estimates of genetic or microbial diversity and may cause misassemblies dur-
252 ing genome reconstruction. Qin et al. (2023) has reported that chimeric sequences
253 may account for more than 10% of raw reads in amplicon datasets. This artifact
254 tends to be most prominent among rare operational taxonomic units (OTUs) or
255 singletons, which are sometimes misinterpreted as novel diversity, further caus-
256 ing the complication of microbial diversity analyses (Gonzalez, Zimmermann, &
257 Saiz-Jimenez, 2004). As such, determining and minimizing PCR-induced chimera
258 formation is vital for improving the quality of mitochondrial genome assemblies,
259 and ensuring the reliability of amplicon sequencing data.

260 2.3 Existing Traditional Approaches for Chimera

261 Detection

Several computational tools have been developed to identify chimeric sequences in NGS datasets. These tools generally fall into two categories: reference-based and de novo approaches. Reference-based chimera detection, also known as database-dependent detection, is one of the earliest and most widely used computational strategies for identifying chimeric sequences in amplicon-based community studies. These methods rely on the comparison of each query sequence against a curated, high-quality database of known, non-chimeric reference sequences (Edgar et al., 2011).

270 On the other hand, the de novo chimera detection, also referred to as reference-
271 free detection, represents an alternative computational paradigm that identifies
272 chimeric sequences without reliance on external reference databases. This method
273 infer chimeras based on internal relationships among the sequences present within
274 the dataset itself, making it particularly advantageous in studies of under explored
275 or taxonomically diverse communities where comprehensive reference databases
276 are unavailable or incomplete (Edgar, 2016; Edgar et al., 2011). The underlying
277 assumption on this method is that during PCR, true biological sequences are
278 generally more abundant as they are amplified early and dominate the read pool,
279 whereas chimeric sequences appear later and are generally less abundant. The
280 de novo approach leverage this abundance hierarchy, treating the most abundant
281 sequences as supposed parents and testing whether less abundant sequences can
282 be reconstructed as mosaics of these templates. Compositional and structural
283 similarity are also evaluated to check whether different regions of a candidate

284 sequence correspond to distinct high-abundance sequences.

285 In practice, many modern bioinformatics pipelines combine both paradigms
286 sequentially: an initial de novo step identifies dataset-specific chimeras, followed
287 by a reference-based pass that removes remaining artifacts relative to established
288 databases (Edgar, 2016). These two methods of detection form the foundation of
289 tools such as UCHIME and later UCHIME2.

290 2.3.1 UCHIME

291 UCHIME is one of the most widely used computational tools for detecting chimeric
292 sequences in amplicon sequencing data, as it serves as a critical quality control
293 step to prevent the misinterpretation of PCR artifacts as novel biological diversity.
294 The algorithm operates by searching for a model (M) where a query (Q) sequence
295 can be perfectly explained as a combination of two parent sequences, denoted as
296 A and B (Edgar et al., 2011).

297 In reference mode, UCHIME divides the query into four chunks and maps
298 them to a trusted chimeric-free database to identify candidate parents. It then
299 constructs a three-way alignment to calculate a score based on “votes.” A “Yes”
300 vote indicates the query aligns with parent A in one region and parent B in an-
301 other, while a “No” vote penalizes the score if the query diverges from the expected
302 chimeric model. In de novo mode, the algorithm operationalizes the abundance
303 skew principle described in Section 2.3. Instead of using an external database,
304 UCHIME dynamically treats the sample’s own high-abundance sequences as a
305 reference database, testing if lower-abundance sequences can be reconstructed as

306 mosaics of these internal ancestors (Edgar et al., 2011).

307 Despite its high sensitivity, UCHIME has inherent limitations rooted in
308 sequence divergence and database quality. The algorithm struggles to detect
309 chimeras formed from parents that are very closely related, specifically when the
310 sequence divergence between parents is less than roughly 0.8%, as the signal-to-
311 noise ratio becomes too low to distinguish a crossover event from sequencing error
312 (Edgar et al., 2011). Furthermore, in reference mode, the accuracy is strictly
313 bound by the completeness of the database; if true parents are absent, the tool
314 may fail to identify the chimera or produce false positives. Similarly, the de novo
315 mode relies on the assumption that parents are present and sufficiently more
316 abundant in the sample, which may not hold true in unevenly amplified samples
317 or complex communities.

318 2.3.2 UCHIME2

319 Building upon the original algorithm, UCHIME2 was developed to address the
320 nuances of high-resolution amplicon sequencing. A key contribution of the
321 UCHIME2 study was the critical re-evaluation of chimera detection benchmarks.
322 In the UCHIME2 paper (Edgar, 2016) and the UCHIME in practice website
323 (Edgar, n.d), the author has noted that the accuracy results reported in the
324 original UCHIME paper were “highly over-optimistic” because they relied on
325 unrealistic benchmark designs where parent sequences were assumed to be 100%
326 known and present. UCHIME2 introduced more rigorous testing (the CHSIMA
327 benchmark), revealing that “fake models,” where a valid biological sequence
328 perfectly mimics a chimera of two other valid sequences, are far more common

329 than previously assumed. This discovery suggests that error-free detection is
330 impossible in principle (Edgar, 2016). Another notable improvement is the in-
331 troduction of multiple application-specific modes that allow users to tailor the
332 algorithm’s performance to the characteristics of their datasets. The following
333 parameter presets: denoised, balanced, sensitive, specific, and high-confidence,
334 enable researchers to optimize the balance between sensitivity and specificity
335 according to the goals of their analysis.

336 However despite these advancements, the practical application of UCHIME2
337 requires caution. The author explicitly advises against using UCHIME2 as
338 a stand-alone tool in standard OTU clustering or denoising pipelines. Using
339 UCHIME2 as an independent filtering step in these workflows is discouraged, as
340 it often results in significantly higher error rates, increasing both false positives
341 (discarding valid sequences) and false negatives (retaining chimeras) (Edgar,
342 2016).

343 2.3.3 CATch

344 As previously mentioned, UCHIME (Edgar et al., 2011) relied on alignment-based
345 sequences in amplicon data. However, researchers soon observed that different al-
346 gorithms often produced inconsistent predictions. A sequence might be identified
347 as chimeric by one tool but classified as non-chimeric by another, resulting in
348 unreliable filtering outcomes across studies.

349 To address these inconsistencies, Mysara, Saeys, Leys, Raes, and Monsieurs
350 (2015) developed the Classifier for Amplicon Tool Chimeras (CATCh), which rep-

351 resents the first ensemble machine learning system designed for chimera detection
352 in 16S rRNA amplicon sequencing. Rather than depending on a single detec-
353 tion strategy, CATCh integrates the outputs of several established tools, includ-
354 ing UCHIME, ChimeraSlayer, DECIPHER, Pintail, and Perseus. The individual
355 scores and binary decisions generated by these tools are used as input features for
356 a supervised learning model. The algorithm employs a Support Vector Machine
357 (SVM) with a Pearson VII Universal Kernel (PUK) to determine optimal weight-
358 ings among the input features and to assign each sequence a probability of being
359 chimeric.

360 Benchmarking in both reference-based and de novo modes demonstrated signif-
361 icant performance improvements. CATCh achieved sensitivities of approximately
362 85 percent in reference-based mode and 92 percent in de novo mode, with corre-
363 sponding specificities of approximately 96 percent and 95 percent. These results
364 indicate that CATCh detected 7 to 12 percent more chimeras than any individual
365 algorithm while maintaining high precision.

366 2.3.4 ChimPipe

367 Among the available tools for chimera detection, ChimPipe is a pipeline developed
368 to identify chimeric sequences such as biological chimeras. It uses both discordant
369 paired-end reads and split-read alignments to improve the accuracy and sensitivity
370 of detecting biological chimeras (Rodriguez-Martin et al., 2017). By combining
371 these two sources of information, ChimPipe achieves better precision than meth-
372 ods that depend on a single type of indicator.

373 The pipeline works with many eukaryotic species that have available genome
374 and annotation data (Rodriguez-Martin et al., 2017). It can also predict multiple
375 isoforms for each gene pair and identify breakpoint coordinates that are useful
376 for reconstructing and verifying chimeric transcripts. Tests using both simulated
377 and real datasets have shown that ChimPipe maintains high accuracy and reliable
378 performance.

379 ChimPipe lets users adjust parameters to fit different sequencing protocols or
380 organism characteristics. Experimental results have confirmed that many chimeric
381 transcripts detected by the tool correspond to functional fusion proteins, demon-
382 strating its utility for understanding chimera biology and its potential applications
383 in disease research (Rodriguez-Martin et al., 2017).

384 **2.4 Machine Learning Approaches for Chimera 385 and Sequence Quality Detection**

386 Traditional chimera detection tools rely primarily on heuristic or alignment-based
387 rules. Recent advances in machine learning (ML) have demonstrated that models
388 trained on sequence-derived features can effectively capture compositional and
389 structural patterns in biological sequences. Although most existing ML systems
390 such as those used for antibiotic resistance prediction, taxonomic classification,
391 or viral identification are not specifically designed for chimera detection, they
392 highlight how data-driven models can outperform similarity-based heuristics by
393 learning intrinsic sequence signatures. In principle, ML frameworks can integrate
394 indicators such as k-mer frequencies, GC-content variation and split-alignment

395 metrics to identify subtle anomalies that may indicate a chimeric origin (Arango
396 et al., 2018; Liang, Bible, Liu, Zou, & Wei, 2020; Ren et al., 2020).

397 **2.4.1 Feature-Based Representations of Genomic Se-**
398 **quences**

399 In genomic analysis, feature extraction converts DNA sequences into numerical
400 representations suitable for ML algorithms. A common approach is k-mer fre-
401 quency analysis, where normalized k-mer counts form the feature vector (Vervier,
402 Mahé, Tournoud, Veyrieras, & Vert, 2015). These features effectively capture lo-
403 cal compositional patterns that often differ between authentic and chimeric reads.

404 In particular, deviations in k-mer profiles between adjacent read segments can
405 serve as a compositional signature of template-switching events. Additional de-
406 scriptors such as GC content and sequence entropy can further distinguish se-
407 quence types; in metagenomic classification and virus detection, k-mer-based fea-
408 tures have shown strong performance and robustness to noise (Ren et al., 2020;
409 Vervier et al., 2015). For chimera detection specifically, abrupt shifts in GC or k-
410 mer composition along a read can indicate junctions between parental fragments.
411 Windowed feature extraction enables models to capture these discontinuities that
412 rule-based algorithms may overlook.

413 Machine learning models can also leverage alignment-derived features such as
414 the frequency of split alignments, variation in mapping quality, and local cover-
415 age irregularities. Split reads and discordant read pairs are classical indicators
416 of genomic junctions and have been formalized in probabilistic frameworks for
417 structural-variant discovery that integrate multiple evidence types (Layer, Hall, &

418 Quinlan, 2014). Similarly, long-read tools such as Sniffles employ split-alignment
419 and coverage anomalies to accurately localize breakpoints (Sedlazeck et al., 2018).
420 Modern aligners such as Minimap2 (Li, 2018) output supplementary (SA tags) and
421 secondary alignments as well as chaining and alignment-score statistics that can
422 be summarized into quantitative predictors for machine-learning models. These
423 alignment-signal features are particularly relevant to PCR-induced mitochondrial
424 chimeras, where template-switching events produce reads partially matching dis-
425 tinct regions of the same or related genomes. Integrating such cues within a
426 supervised-learning framework enables artifact detection even in datasets lacking
427 complete or perfectly assembled references.

428 A further biologically grounded descriptor is the length of microhomology at
429 putative junctions. Microhomology refers to short, shared sequences, often in the
430 range of a few to tens of base pairs that are near breakpoints where template-
431 switching events typically happen. Studies of double strand break repair and
432 structural variation have demonstrated that the length of microhomology corre-
433 lates with the likelihood of microhomology-mediated end joining (MMEJ) or fork-
434 stalled template-switching pathways (Sfeir & Symington, 2015). In the context of
435 PCR-induced chimeras, template switching during amplification often leaves short
436 identical sequences at the junction of two concatenated fragments. Quantifying
437 the longest exact suffix–prefix overlap at each candidate breakpoint thus provides
438 a mechanistic signature of chimerism and complements both compositional (k-
439 mer) and alignment (SA count) features.

440 2.5 Synthesis of Chimera Detection Approaches

441 To provide an integrated overview of the literature discussed in this chapter, Ta-
442 ble 2.1 summarizes the major chimera detection studies, their methodological
443 approaches, and their known limitations.

Table 2.1: Comparison of Chimera Detection Methods

Methods	Approach	Limitations
Reference-based Chimera Detection	Compares query sequences against curated, non-chimeric reference databases; identifies mosaic sequences by evaluating similarity to known templates.	Depends heavily on completeness and quality of reference databases; often fails when novel taxa or missing parent sequences are present; reduced accuracy for low-divergence chimeras.
De novo Chimera Detection	Identifies chimeras using only internal dataset relationships; relies on abundance patterns and compositional similarity; reconstructs sequences as mosaics of high-abundance parents.	Assumes true sequences are more abundant—fails when amplification bias distorts abundance; struggles with evenly abundant parental sequences; can misclassify highly similar true variants.
UCHIME	Alignment-based chimera detection; segments query sequence, identifies parent candidates, performs 3-way alignment, and computes chimera scores; supports both reference-based and de novo modes.	Accuracy inflated in original benchmarks; suffers under incomplete databases; poor performance on low-divergence chimeras; sensitive to sequencing errors; misclassifies when parents are missing.
UCHIME2	Improved initial UCHIME benchmarking; offers multiple sensitivity/specificity modes; more robust with incomplete references; higher sensitivity.	Cannot achieve perfect accuracy due to “perfect fake models”; genuine variants may be indistinguishable from artificial recombinants; theoretical detection limit remains.
CATCh	First ML ensemble tool for 16S chimera detection; integrates outputs of UCHIME, ChimeraSlayer, DECIPHER, Pintail, Perseus via SVM classifier; significantly improves sensitivity and specificity.	Depends on performance of underlying tools; ML model limited to features they output; ensemble can still misclassify in datasets with extreme novelty or low coverage.
ChimPipe	Pipeline for detecting fusion genes and transcript-derived chimeras in RNA-seq; uses discordant paired-end reads and split-alignments; predicts isoforms and breakpoint coordinates.	Designed for RNA-seq, not amplicons; needs high-quality genome and annotation; computationally heavier; limited to organisms with reference genomes.

444 Across existing studies, no single approach reliably detects all forms of chimeric
445 sequences, particularly those generated by PCR-induced template switching in
446 mitochondrial genomes. Reference-based tools perform poorly when parental se-
447 quences are absent; de novo methods rely strongly on abundance assumptions;
448 alignment-based systems show reduced sensitivity to low-divergence chimeras; and
449 ensemble methods inherit the limitations of their component algorithms. RNA-
450 seq-oriented pipelines likewise do not generalize well to organelle data. Although
451 machine learning approaches offer promising feature-based detection, they are
452 rarely applied to mitochondrial genomes and are not trained specifically on PCR-
453 induced organelle chimeras. These limitations indicate a clear research gap: the
454 need for a specialized, feature-driven classifier tailored to mitochondrial PCR-
455 induced chimeras that integrates k-mer composition, split-alignment signals, and
456 micro-homology features to achieve more accurate detection than current heuristic
457 or alignment-based tools.

⁴⁵⁸ Chapter 3

⁴⁵⁹ Research Methodology

⁴⁶⁰ This chapter outlines the steps involved in completing the study, including data
⁴⁶¹ gathering, generating simulated mitochondrial Illumina reads, preprocessing and
⁴⁶² indexing the data, developing a feature extraction pipeline to extract key features,
⁴⁶³ applying machine learning algorithms for chimera detection, and validating and
⁴⁶⁴ comparing model performance.

⁴⁶⁵ 3.1 Research Activities

⁴⁶⁶ As illustrated in Figure 3.1, this study carried out a sequence of procedures to
⁴⁶⁷ detect PCR-induced chimeric reads in mitochondrial genomes. The process began
⁴⁶⁸ with collecting a mitochondrial reference sequence of *Sardinella lemuru* from the
⁴⁶⁹ National Center for Biotechnology Information (NCBI) database, which was used
⁴⁷⁰ as a reference for generating simulated clean and chimeric reads. These reads
⁴⁷¹ were subsequently indexed and mapped. The resulting collections then passed

472 through a feature extraction pipeline that extracted k-mer profiles, supplementary
473 alignment (SA) features, and microhomology information to prepare the data for
474 model construction. The machine learning model was trained using the processed
475 input, and its precision and accuracy were assessed. It underwent tuning until it
476 reached the desired performance threshold, after which it proceeded to validation
477 and will undergo testing.

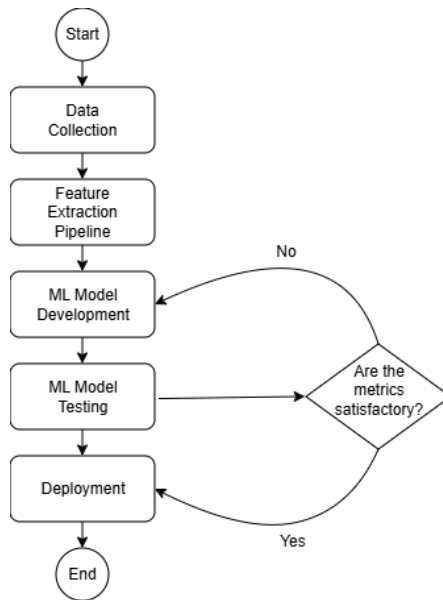


Figure 3.1: Process Diagram of Special Project

478 3.1.1 Data Collection

479 The mitochondrial genome reference sequence of *S. lemuru* was obtained from the
480 NCBI database (accession number NC_039553.1) in FASTA format. This sequence
481 served as the basis for generating simulated reads for model development.

482 This step was scheduled to begin in the first week of November 2025 and
483 expected to be completed by the end of that week, with a total duration of ap-

484 proximately one (1) week.

485 Data Preprocessing

486 To reduce manual repetition, all steps in the simulation and preprocessing pipeline
487 were executed using a custom script in Python (Version 3.11). The script runs
488 each stage, including read simulation, reference indexing, mapping, and alignment
489 processing, in a fixed sequence.

490 Sequencing data were simulated from the NCBI reference genome using `wgsim`
491 (Version 1.13). First, a total of 10,000 paired-end fragments were simulated,
492 producing 20,000 reads (10,000 forward and 10,000 reverse) from the the original
493 reference (`original_reference.fasta`) and and designated as clean reads using
494 the command:

```
495 wgsim -1 150 -2 150 -r 0 -R 0 -X 0 -e 0.001 -N 10000 \  
496           original_reference.fasta ref1.fastq ref2.fastq
```

497 The command parameters are as follows:

- 498 • `-1` and `-2`: read lengths of 150 base pairs for each paired-end read.
- 499 • `-r`, `-R`, `-X`: mutation rate, fraction of indels, and indel extension probability,
500 all set to a default value of 0.
- 501 • `-e`: base error rate, set to 0.001 to simulate realistic sequencing errors.
- 502 • `-N`: number of read pairs, set to 10,000.

503 Chimeric sequences were then generated from the same NCBI reference using a
504 separate Python script. Two non-adjacent segments were randomly selected such
505 that their midpoint distances fell within specified minimum and maximum thresh-
506 olds. The script attempts to retain microhomology, or short identical sequences
507 at segment junctions, to mimic PCR-induced template switching. The resulting
508 chimeras were written to `chimera_reference.fasta`, with headers recording seg-
509 ment positions and microhomology length. The `chimera_reference.fasta` was
510 processed with `wgsim` to simulate 10,000 paired-end fragments, generating 20,000
511 chimeric reads (10,000 forward reads in `chimeric1.fastq` and 10,000 reverse reads
512 in `chimeric2.fastq`) using the command format.

513 Next, a `minimap2` index of the reference genome was created using:

```
514 minimap2 -d ref.mmi original_reference.fasta
```

515 Minimap2 (Version 2.28) is a tool used to map reads to a reference genome.
516 The index `ref.mmi` of the original reference sequence is required by `minimap2` for
517 efficient read mapping. Mapping allows extraction of alignment features from each
518 read, which were used as input for the machine learning model. The simulated
519 clean and chimeric reads were then mapped to the reference index as follows:

```
520 minimap2 -ax sr -t 8 ref.mmi ref1.fastq ref2.fastq > clean.sam
```

```
521 minimap2 -ax sr -t 8 ref.mmi \  
522 chimeric1.fastq chimeric2.fastq > chimeric.sam
```

523 Here, `-ax sr` specifies short-read alignment mode, and `-t 8` uses 8 CPU

524 threads. The resulting clean and chimeric SAM files contain the alignment posi-
525 tions of each read relative to the original reference genome.

526 The SAM files were then converted to BAM format, sorted, and indexed using
527 `samtools` (Version 1.20):

```
528 samtools view -bS clean.sam -o clean.bam  
529 samtools view -bS chimeric.sam -o chimeric.bam  
530  
531 samtools sort clean.bam -o clean.sorted.bam  
532 samtools index clean.sorted.bam  
533  
534 samtools sort chimeric.bam -o chimeric.sorted.bam  
535 samtools index chimeric.sorted.bam
```

536 BAM files are the compressed binary version of SAM files, which enables faster
537 processing and reduced storage. Sorting arranges reads by genomic coordinates,
538 and indexing allows detection of SA as a feature for the machine learning model.

539 The total number of simulated reads was expected to be 40,000. The final col-
540 lection of reads contained 19,984 clean reads and 20,000 chimeric reads (39,984 en-
541 tries in total), providing a roughly balanced distribution between the two classes.
542 After alignment with `minimap2`, only 19,984 clean reads remained because un-
543 mapped reads were not included in the BAM file. Some sequences failed to align
544 due to the 5% error rate defined during `wgsim` simulation, which produced mis-
545 matches that caused certain reads to fall below the aligner's matching threshold.

546 This whole process is scheduled to start in the second week of November 2025

547 and is expected to be completed by the last week of November 2025, with a total
548 duration of approximately three (3) weeks.

549 **3.1.2 Feature Extraction Pipeline**

550 A feature extraction pipeline will be developed and implemented to extract the
551 necessary analytical features. This pipeline will function as a reproducible and
552 modular workflow that accepts FASTQ and BAM/SAM file inputs, processes them
553 using tools such as `samtools` and `jellyfish` (Version 2.3.1), and produces tabular
554 feature matrices (TSV) for downstream machine learning. To ensure correctness
555 and adherence to best practices, bioinformatics experts at the PGC Visayas will
556 be consulted to validate the pipeline design, feature extraction logic, and overall
557 data integrity. This stage of the study is scheduled to begin in the first week of
558 January 2026 and conclude by the last week of February 2026, with an estimated
559 total duration of approximately two (2) months.

560 The feature extraction pipeline focuses on three principal features from the
561 simulated and aligned sequencing data: (1) supplementary alignment flag (SA
562 count), (2) k-mer composition difference between read segments, and (3) micro-
563 homology length at potential junctions. Each of these features captures a distinct
564 biological or computational signature associated with PCR-induced chimeras.

565 **Supplementary Alignment Flag**

566 Supplementary alignment information will be assessed using the mapped and
567 sorted BAM files (`clean.sorted.bam` and `chimeric.sorted.bam`) generated

568 from the data preprocessing stage. Alignment summaries will be checked using
569 `samtools flagstat` to obtain preliminary quality-control statistics, including
570 counts of primary, secondary, and supplementary (SA) alignments.

571 Both BAM files will be converted to SAM format for detailed inspection of
572 reads in each file:

```
573 samtools view -h clean.sorted.bam -o clean.sorted.sam  
574 samtools view -h chimeric.sorted.bam -o chimeric.sorted.sam
```

575 The SAM output will be checked for reads containing the SA:Z flag, as it
576 denotes supplementary alignments. Reads exhibiting these or substantial soft-
577 clipped regions will be considered strong candidates for chimeric artifacts. A
578 custom Python script would be created to extract the alignment-derived features
579 and relevant metadata including mapping quality, SAM flag information, CIGAR-
580 based clipping, and alignment coordinates. These extracted attributes would then
581 be organized and compiled into a TSV (.tsv) file.

582 K-mer Composition Difference

583 Chimeric reads often comprise fragments from distinct genomic regions, resulting
584 in a compositional discontinuity between segments. Comparing k-mer frequency
585 profiles between the left and right halves of a read allows detection of such abrupt
586 compositional shifts, independent of alignment information. This will be obtained
587 using Jellyfish, a fast k-mer counting software. For each read, the sequence will
588 be divided into two segments, either at the midpoint or at empirically determined
589 breakpoints inferred from supplementary alignment data, to generate left and right

590 sequence segments. Jellyfish will then compute k-mer frequency profiles (with $k =$
591 5 or 6) for each segment. The resulting k-mer frequency vectors will be normalized
592 and compared using distance metrics such as cosine similarity or Jensen–Shannon
593 divergence to quantify compositional disparity between the two halves of the same
594 read. The resulting difference scores will be stored in a structured TSV file.

595 Microhomology Length

596 The microhomology length was computed as part of the feature extraction
597 pipeline. For each aligned read in the BAM files, the script first inferred a
598 breakpoint using the function `infer_breakpoint`, which represents a junction
599 between two segments. Breakpoints were determined primarily from soft-clipping
600 patterns. If no soft clips were present, SA tags were used to identify potential
601 alignment discontinuities.

602 Once a breakpoint was established, the script scanned a ± 40 base pair window
603 surrounding the breakpoint and used the function `longest_suffix_prefix_overlap`
604 to identify the longest exact suffix-prefix overlap between the left and right read
605 segments. This overlap, which represents consecutive bases shared at the junc-
606 tion, was recorded as the microhomology length. Additionally, the GC content
607 of the overlapping sequence was calculated using the function `gc_content`, which
608 counts guanine (G) and cytosine (C) bases within the detected microhomology
609 and divides by the total length, yielding a proportion between 0 and 1.

610 Short microhomologies, typically 3-20 base pairs in length, are recognized sig-
611 natures of PCR-induced template switching and can promote template recombi-
612 nation (Peccoud et al., 2018). Each read was annotated after capturing both the

613 length and GC content of microhomology.

614 3.1.3 Machine Learning Model Development

615 After feature extraction, the per-read feature matrices for clean and chimeric
616 reads were merged into a single dataset. Each row corresponded to one paired-
617 end read, and columns encoded alignment-structure features (e.g., supplementary
618 alignment count and spacing between segments), CIGAR-derived soft-clipping
619 statistics (e.g., left and right soft-clipped length, total clipped bases), k-mer com-
620 position discontinuity between read segments, and microhomology descriptors
621 near candidate junctions. The resulting feature set was restricted to quantities
622 that can be computed from standard BAM/FASTQ files in typical mitochondrial
623 sequencing workflows.

624 The labelled dataset was randomly partitioned into training (80%) and test
625 (20%) subsets using stratified sampling to preserve the 1:1 ratio of clean to
626 chimeric reads. Model development and evaluation were implemented in Python
627 (Version 3.11) using the `scikit-learn`, `xgboost`, `lightgbm`, and `catboost` li-
628 braries. A broad panel of classification algorithms was then benchmarked on the
629 training data to obtain a fair comparison of different model families under identical
630 feature conditions. The panel included: a trivial dummy classifier, L2-regularized
631 logistic regression, a calibrated linear support vector machine (SVM), k -nearest
632 neighbours, Gaussian Naïve Bayes, decision-tree ensembles (Random Forest, Ex-
633 tremely Randomized Trees, and Bagging with decision trees), gradient boosting
634 methods (Gradient Boosting, XGBoost, LightGBM, and CatBoost), and a shallow
635 multilayer perceptron (MLP).

636 For each model, five-fold stratified cross-validation was performed on the train-
637 ing set. In every fold, four-fifths of the data were used for fitting and the remaining
638 one-fifth for validation. Mean cross-validation accuracy, precision, recall, F1-score
639 for the chimeric class, and area under the receiver operating characteristic curve
640 (ROC–AUC) were computed to summarize performance and rank candidate meth-
641 ods. This baseline screen allowed comparison of linear, probabilistic, neural, and
642 ensemble-based approaches and identified tree-based ensemble and boosting mod-
643 els as consistently strong performers relative to simpler baselines.

644 **3.1.4 Model Benchmarking, Hyperparameter Optimiza-
645 tion, and Evaluation**

646 Model selection and refinement proceeded in two stages. First, the cross-validation
647 results from the broad panel were used to identify a subset of competitive mod-
648 els for more detailed optimization. Specifically, ten model families were carried
649 forward: L2-regularized logistic regression, calibrated linear SVM, Random For-
650 est, ExtraTrees, Gradient Boosting, XGBoost, LightGBM, CatBoost, Bagging
651 with decision trees, and a shallow MLP. This subset spans both linear and non-
652 linear decision boundaries, but emphasizes ensemble and boosting methods, which
653 showed superior F1 and ROC–AUC in the initial benchmark.

654 Second, hyperparameter optimization was conducted for each of the ten se-
655 lected models using randomized search with five-fold stratified cross-validation
656 (`RandomizedSearchCV`). For tree-based ensembles, the search space included the
657 number of trees, maximum depth, minimum samples per split and leaf, and the
658 fraction of features considered at each split. For boosting methods, key hyper-

659 parameters such as the number of boosting iterations, learning rate, tree depth,
660 subsampling rate, and column subsampling rate were tuned. For the MLP, the
661 number and size of hidden layers, learning rate, and L_2 regularization strength
662 were varied. In all cases, the primary optimisation criterion was the F1-score of
663 the chimeric class, averaged across folds.

664 For each model family, the hyperparameter configuration with the highest
665 mean cross-validation F1-score was selected as the best-tuned estimator. These
666 tuned models were then refitted on the full training set and evaluated once on the
667 held-out test set to obtain unbiased estimates of performance. Test-set metrics in-
668 cluded accuracy, precision, recall, F1-score for the chimeric class, and ROC–AUC.
669 Confusion matrices and ROC curves were generated for the top-performing mod-
670 els to characterise common error modes, such as false negatives (missed chimeric
671 reads) and false positives (clean reads incorrectly labelled as chimeric). The final
672 model or small set of models for downstream interpretation was chosen based on
673 a combination of test-set F1-score, ROC–AUC, and practical considerations such
674 as model complexity and ease of deployment within a feature extraction pipeline.

675 3.1.5 Feature Importance and Interpretation

676 To relate model decisions to biologically meaningful signals, feature-importance
677 analyses were performed on the best-performing tree-based models. Two comple-
678 mentary approaches were used. First, built-in importance measures from ensemble
679 methods (e.g., split-based importances in Random Forest and Gradient Boosting)
680 were examined to obtain an initial ranking of features based on their contribution
681 to reducing impurity. Second, model-agnostic permutation importance was com-

682 puted on the test set by repeatedly permuting each feature column while keeping
683 all others fixed and measuring the resulting decrease in F1-score. Features whose
684 permutation led to a larger performance drop were interpreted as more influential
685 for chimera detection.

686 For interpretability, individual features were grouped into four conceptual
687 families: (i) supplementary alignment and alignment-structure features (e.g., SA
688 count, spacing between alignment segments, strand consistency), (ii) CIGAR-
689 derived soft-clipping features (e.g., left and right soft-clipped length, total clipped
690 bases), (iii) k-mer composition discontinuity features (e.g., cosine distance and
691 Jensen–Shannon divergence between k-mer profiles of read segments), and (iv) mi-
692 crohomology descriptors (e.g., microhomology length and local GC content around
693 putative breakpoints). Aggregating permutation importance scores within each
694 family allowed assessment of which biological signatures contributed most strongly
695 to the classifier’s performance. This analysis provided a basis for interpreting the
696 trained models in terms of known mechanisms of PCR-induced template switching
697 and for identifying which alignment- and sequence-derived cues are most informa-
698 tive for distinguishing chimeric from clean mitochondrial reads.

699 **3.1.6 Validation and Testing**

700 Validation will involve both internal and external evaluations. Internal valida-
701 tion was achieved through five-fold cross-validation on the training data to verify
702 model generalization and reduce variance due to random sampling. External vali-
703 dation will be achieved through testing on the 20% hold-out dataset derived from
704 the simulated reads, which will be an unbiased benchmark to evaluate how well

705 the trained models generalized to unseen data. All feature extraction and prepro-
706 cessing steps were performed using the same feature extraction pipeline to ensure
707 consistency and comparability across validation stages.

708 Comparative evaluation was performed across all candidate algorithms, in-
709 cluding a trivial dummy classifier, L2-regularized logistic regression, a calibrated
710 linear SVM, k-nearest neighbours, Gaussian Naïve Bayes, decision-tree ensembles,
711 gradient boosting methods, and a shallow MLP. This evaluation determined which
712 models demonstrated the highest predictive performance and computational effi-
713 ciency under identical data conditions. Their metrics were compared to identify
714 which algorithms were most suitable for further refinement.

715 3.1.7 Documentation

716 Comprehensive documentation was maintained throughout the study to ensure
717 transparency and reproducibility. All stages of the research, including data gath-
718 ering, preprocessing, feature extraction, model training, and validation, were sys-
719 tematically recorded in a `.README` file in the GitHub repository. For each ana-
720 lytical step, the corresponding parameters, software versions, and command line
721 scripts were documented to enable exact replication of results.

722 The repository structure followed standard research data management prac-
723 tices, with clear directories for datasets and scripts. Computational environments
724 were standardized using Conda, with an environment file (`environment.arm.yml`)
725 specifying dependencies and package versions to maintain consistency across sys-
726 tems.

₇₂₇ For manuscript preparation and supplementary materials, Overleaf (L^AT_EX)
₇₂₈ was used to produce publication-quality formatting and consistent referencing. f

₇₂₉ 3.2 Calendar of Activities

₇₃₀ Table 3.1 presents the project timeline in the form of a Gantt chart, where each
₇₃₁ bullet point corresponds to approximately one week of planned activity.

Table 3.1: Timetable of Activities

Activities (2025)	Nov	Dec	Jan	Feb	Mar	Apr	May
Data Collection and Simulation	• • •						
Feature Extraction Pipeline			• • •	• • •			
Machine Learning Development			••	• • •	• • •	••	
Testing and Validation						••	• • •
Documentation	• • •	• • •	• • •	• • •	• • •	• • •	• • •

732 Chapter 4

733 Results and Discussion

734 4.1 Descriptive Analysis of Features

735 This chapter presents the performance of the proposed feature set and machine-
736 learning models for detecting PCR-induced chimeric reads in simulated mitochon-
737 drial Illumina data. We first describe the behaviour of the main features, then
738 compare baseline classifiers, assess the effect of hyperparameter tuning, and fi-
739 nally analyse feature importance in terms of individual variables and biologically
740 motivated feature families.

741 The final dataset contained 31 986 reads for training and 7 997 reads for testing,
742 with classes balanced (approximately 4 000 clean and 4 000 chimeric reads in the
743 test split).

744 4.1.1 Univariate Distributions

745 The kernel density plots in Figures 4.1a–4.1f collectively show that alignment-
746 based features provide the strongest separation between clean and chimeric reads.
747 The distribution of `sa_count` (Figure 4.1a) is distinctly bimodal, with clean reads
748 concentrated near zero and chimeric reads peaking around one, reflecting the
749 frequent presence of supplementary alignments in chimeras. A similar pattern of
750 clear separation is observed in `softclip_left` and `softclip_right` (Figures 4.1c
751 and 4.1d), where clean reads cluster tightly at zero while chimeric reads display
752 broad, long-tailed distributions, consistent with extensive soft clipping when
753 a read spans multiple genomic locations. In contrast, `microhomology_length`
754 (Figure 4.1b) shows substantial overlap between classes, with both distribu-
755 tions sharply concentrated near zero and exhibiting smaller secondary peaks
756 at short integer lengths, indicating limited discriminative value under the sim-
757 ulated conditions. Finally, the k-mer-based features `kmer_js_divergence` and
758 `kmer_cosine_diff` (Figures 4.1e and 4.1f) exhibit highly overlapping, multimodal
759 distributions with both classes peaking near 1.0; although chimeric reads appear
760 slightly less concentrated at the highest similarity values, the separation is weak
761 overall.

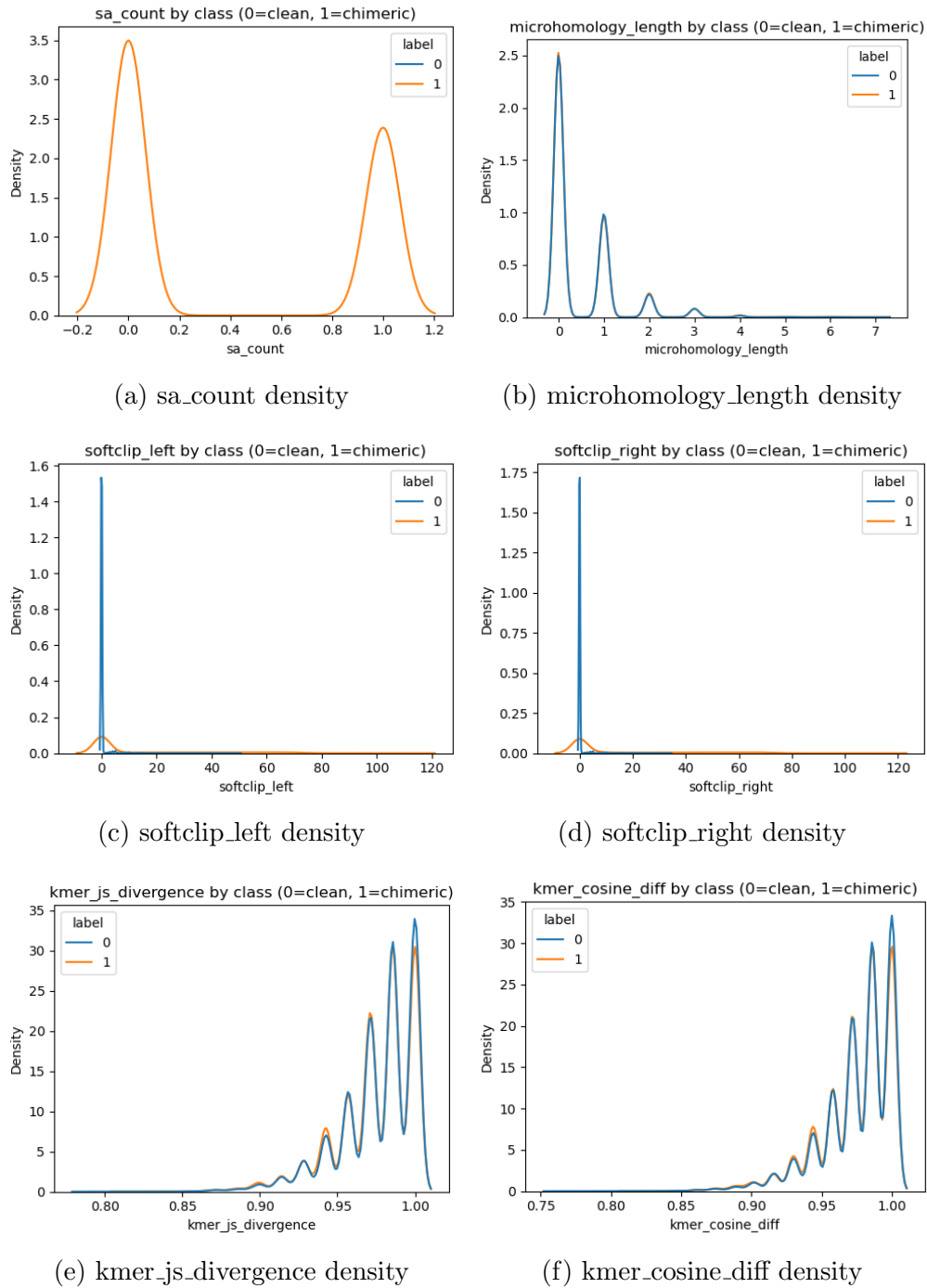


Figure 4.1: Kernel density plots of six key features comparing clean and chimeric reads.

762 4.2 Baseline Classification Performance

763 Table 4.1 summarises the performance of eleven classifiers trained on the engi-
764 neered feature set using five-fold cross-validation and evaluated on the held-out
765 test set. All models were optimised using default hyperparameters, without ded-
766 icated tuning.

767 The dummy baseline, which always predicts the same class regardless of the
768 input features, achieved an accuracy of 0.50 and test F1-score of 0.67. This re-
769 flects the balanced class distribution and provides a lower bound for meaningful
770 performance.

771 Across other models, test F1-scores clustered in a narrow band between ap-
772 proximately 0.74 and 0.77 and ROC–AUC values between 0.82 and 0.84. Gradi-
773 ent boosting, CatBoost, LightGBM, XGBoost, bagging trees, random forest, and
774 multilayer perceptron (MLP) all produced very similar scores, with CatBoost and
775 gradient boosting slightly ahead (test F1 \approx 0.77, ROC–AUC \approx 0.84). Linear
776 models (logistic regression and calibrated linear SVM) performed only marginally
777 worse (test F1 \approx 0.74), while Gaussian Naive Bayes lagged behind with substan-
778 tially lower F1 (\approx 0.65) despite very high precision for the chimeric class.

Table 4.1: Performance of baseline classifiers on the held-out test set.

model	test_accuracy	test_precision	test_recall	test_f1	test_roc_auc
dummy_baseline	0.500000	0.500000	1.000000	0.667000	0.500000
logreg_l2	0.789000	0.945000	0.614000	0.744000	0.821000
linear_svm_calibrated	0.789000	0.945000	0.614000	0.744000	0.820000
random_forest	0.788000	0.894000	0.654000	0.755000	0.834000
extra_trees	0.788000	0.901000	0.647000	0.753000	0.824000
gradient_boosting	0.802000	0.936000	0.648000	0.766000	0.840000
xgboost	0.800000	0.929000	0.650000	0.765000	0.839000
lightgbm	0.799000	0.926000	0.650000	0.764000	0.838000
catboost	0.803000	0.936000	0.650000	0.767000	0.839000
knn	0.782000	0.892000	0.642000	0.747000	0.815000
gaussian_nb	0.741000	0.996000	0.483000	0.651000	0.819000
bagging_trees	0.792000	0.900000	0.657000	0.760000	0.837000
mlp	0.789000	0.931000	0.625000	0.748000	0.819000

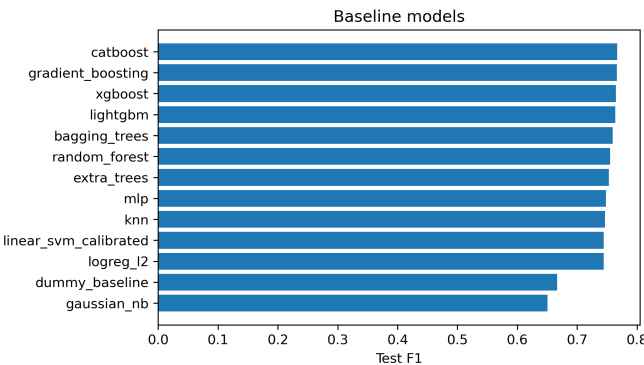


Figure 4.2: Test F1 of all baseline classifiers, showing that no single model clearly dominates and several achieve comparable performance.

779 4.3 Effect of Hyperparameter Tuning

780 To assess whether performance could be improved further, ten model families un-
 781 derwent randomised hyperparameter search (Chapter 3). The tuned metrics are
 782 summarised in Table 4.2. Overall, tuning yielded modest but consistent gains for
 783 tree-based ensembles and boosting methods, while leaving linear models essen-

784 tially unchanged or slightly worse.

785 CatBoost, gradient boosting, LightGBM, XGBoost, random forest, bagging
786 trees, and MLP all experienced small increases in test F1 (typically $\Delta F1 \approx 0.002 -$
787 0.009) and ROC–AUC (up to $\Delta AUC \approx 0.008$). After tuning, CatBoost remained
788 the best performer with test accuracy 0.802, precision 0.924, recall 0.658, F1-score
789 0.769, and ROC–AUC 0.844. Gradient boosting achieved almost identical perfor-
790 mance (F1 0.767, AUC 0.843). Random forest and bagging trees also improved
791 to F1 scores around 0.763 with AUC ≈ 0.842 .

Table 4.2: Performance of tuned classifiers on the held-out test set.

model	test_accuracy	test_precision	test_recall	test_f1	test_roc_auc
logreg_l2_tuned	0.788000	0.946000	0.612000	0.743000	0.818000
linear_svm_calibrated_tuned	0.788000	0.944000	0.612000	0.743000	0.818000
random_forest_tuned	0.797000	0.915000	0.655000	0.763000	0.842000
extra_trees_tuned	0.794000	0.910000	0.652000	0.760000	0.837000
gradient_boosting_tuned	0.802000	0.928000	0.654000	0.767000	0.843000
xgboost_tuned	0.799000	0.922000	0.653000	0.765000	0.839000
lightgbm_tuned	0.801000	0.930000	0.651000	0.766000	0.842000
catboost_tuned	0.802000	0.924000	0.658000	0.769000	0.844000
bagging_trees_tuned	0.798000	0.922000	0.650000	0.763000	0.842000
mlp_tuned	0.790000	0.934000	0.625000	0.749000	0.821000

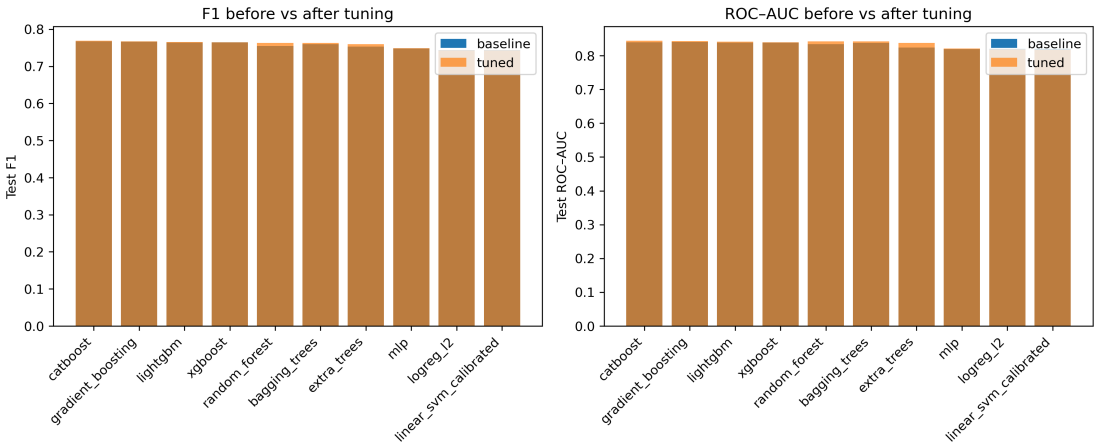


Figure 4.3: Comparison of test F1 (left) and ROC–AUC (right) for baseline and tuned models. Hyperparameter tuning yields small but consistent gains, particularly for tree-based ensembles.

792 Because improvements are small and within cross-validation variability, we
 793 interpret tuning as stabilising and slightly refining the models rather than funda-
 794 mentally altering their behaviour or their relative ranking.

795 4.4 Detailed Evaluation of Representative Mod- 796 els

797 For interpretability and diversity, four tuned models were selected for deeper
 798 analysis: CatBoost (best-performing boosted tree), scikit-learn gradient boost-
 799 ing (canonical gradient-boosting implementation), random forest (non-boosted
 800 ensemble baseline), and L2-regularised logistic regression (linear baseline). All
 801 models were trained on the engineered feature set and evaluated on the same
 802 held-out test data.

803 4.4.1 Confusion Matrices and Error Patterns

804 Classification reports and confusion matrices for the four models reveal consistent
805 patterns. CatBoost and gradient boosting both reached overall accuracy of ap-
806 proximately 0.80 with similar macro-averaged F1 scores (~ 0.80). For CatBoost,
807 precision and recall for clean reads were 0.73 and 0.95, respectively, while for
808 chimeric reads they were 0.92 and 0.66 (F1 = 0.77). Gradient boosting showed
809 nearly identical trade-offs.

810 Random forest attained slightly lower accuracy (0.80) and chimeric F1 (0.76),
811 whereas logistic regression achieved the lowest accuracy among the four (0.79)
812 and chimeric F1 (0.74), although it provided the highest chimeric precision (0.95)
813 at the cost of lower recall (0.61).

814 Across all models, errors were asymmetric. False negatives (chimeric reads
815 predicted as clean) were more frequent than false positives. For example, CatBoost
816 misclassified 1 369 chimeric reads as clean but only 215 clean reads as chimeric.
817 This pattern indicates that the models are conservative: they prioritise avoiding
818 spurious chimera calls at the expense of missing some true chimeras. Depending on
819 downstream application, alternative decision thresholds or cost-sensitive training
820 could be explored to adjust this balance.

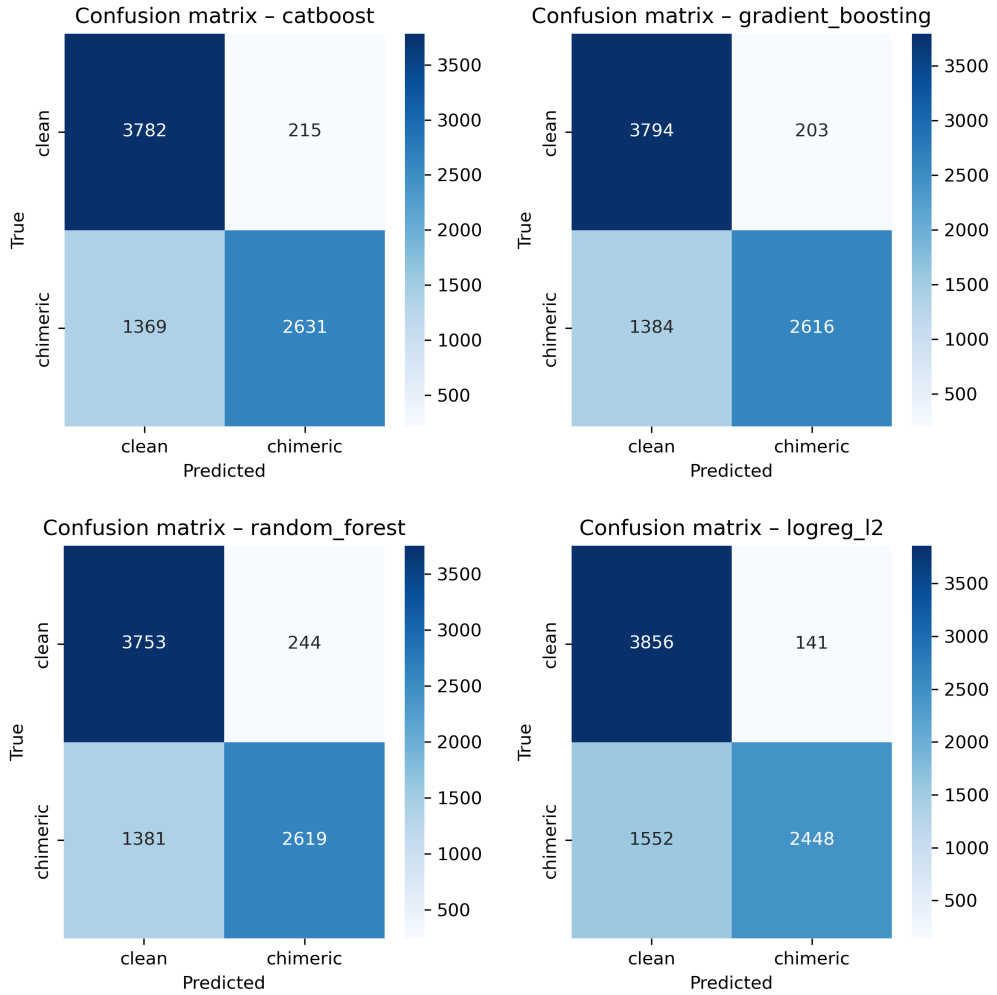


Figure 4.4: Confusion matrices for the four representative models on the held-out test set. All models show more false negatives (chimeric reads called clean) than false positives.

821 4.4.2 ROC and Precision–Recall Curves

822 Receiver operating characteristic (ROC) and precision–recall (PR) curves (Fig-
 823 ure 4.5) further support the similarity among the top models. The three tree-based
 824 ensembles (CatBoost, gradient boosting, random forest) achieved ROC–AUC val-
 825 ues of approximately 0.84 and average precision (AP) around 0.88. Logistic re-

826 gression performed slightly worse ($AUC \approx 0.82$, $AP \approx 0.87$) but still substantially
827 better than random guessing.

828 The PR curves show that precision remains above 0.9 across a broad range
829 of recall values (up to roughly 0.5–0.6), after which precision gradually declines.
830 This behaviour indicates that the models can assign very high confidence to a
831 subset of chimeric reads, while more ambiguous reads can only be recovered by
832 accepting lower precision.

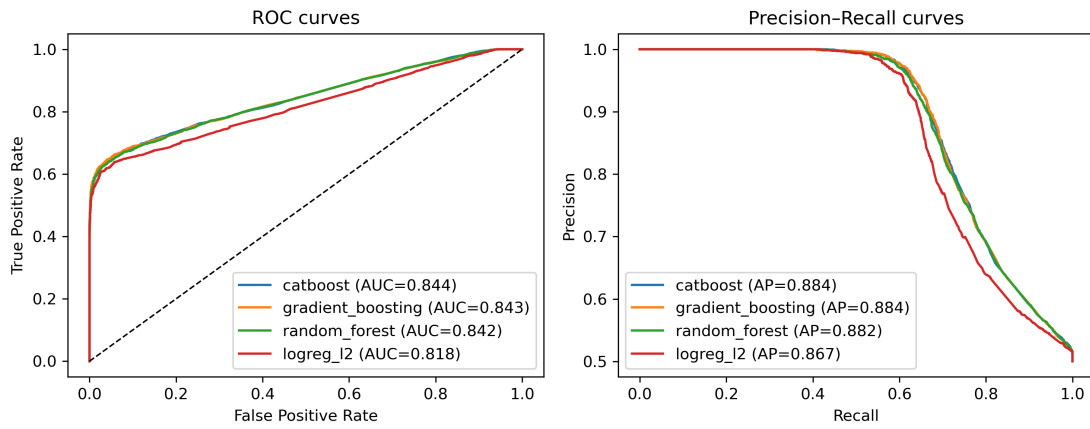


Figure 4.5: ROC (left) and precision–recall (right) curves for the four representative models on the held-out test set. Tree-based ensembles cluster closely, with logistic regression performing slightly but consistently worse.

833 **4.5 Feature Importance and Biological Interpre-**
834 **tation**

835 **4.5.1 Permutation Importance of Individual Features**

836 To understand how each classifier made predictions, feature importance was quan-
837 tified using permutation importance. In this approach, the values of a single fea-
838 ture are randomly shuffled, and the resulting drop in F_1 score (ΔF_1) reflects how
839 strongly the model depends on that feature. Greater decreases in F_1 indicate
840 stronger reliance on that feature. This analysis was applied to four representa-
841 tive models: CatBoost, Gradient Boosting, Random Forest, and L_2 -regularized
842 Logistic Regression.

843 As shown in Figure 4.6, the total number of clipped bases consistently pro-
844 vides a strong predictive signal, particularly in Random Forest, Gradient Boosting,
845 and L_2 -regularized Logistic Regression. CatBoost differs by assigning the highest
846 importance to k-mer divergence metrics such as `kmer_js_divergence`, which cap-
847 ture subtle sequence changes resulting from structural variants or PCR-induced
848 chimeras. Soft-clipping features (`softclip_left` and `softclip_right`) provide
849 additional context around breakpoints, complementing these primary signals in
850 all models except Gradient Boosting. L_2 -regularized Logistic Regression relies
851 more on alignment-based split-read metrics when breakpoints are simple, but it is
852 less effective at detecting complex rearrangements that introduce novel sequences.

853 Overall, these results indicate that accurate detection of chimeric reads relies
854 on both alignment-based signals and k-mer compositional information. Explicit

855 microhomology features contribute minimally in this analysis, and combining both
 856 alignment-based and sequence-level features enhances model sensitivity and speci-
 857 ficity.

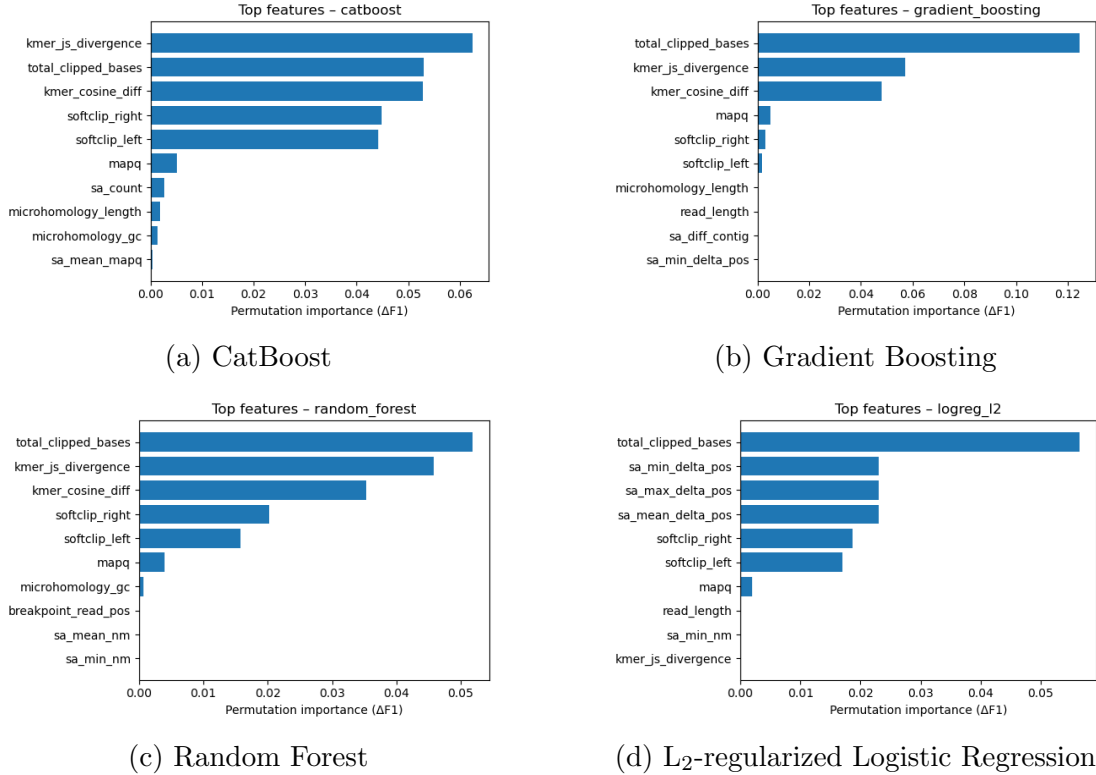


Figure 4.6: Permutation-based feature importance for four representative classifiers. Clipping and k-mer composition features are generally the strongest predictors, whereas microhomology and other alignment metrics contribute minimally.

858 4.5.2 Feature Family Importance

859 To evaluate the contribution of broader biological signals, features were
 860 grouped into five families: SA_structure (supplementary alignment and seg-
 861 ment metrics, e.g., has_sa, sa_count, sa_min_delta_pos, sa_mean_nm), Clipping
 862 (softclip_left, softclip_right, total_clipped_bases, breakpoint_read_pos),

863 Kmer_jump (`kmer_cosine_diff`, `kmer_js_divergence`), Micro_homology, and
864 Other (e.g., `mapq`).

865 Aggregated analyses reveal consistent patterns across models. In CatBoost,
866 the Clipping family has the largest cumulative contribution (0.14), followed
867 by Kmer_jump (0.12), with Other features contributing modestly (0.005) and
868 SA_structure (0.003) and Micro_homology (0.003) providing minimal predictive
869 power. Gradient Boosting shows a similar trend, with Clipping (0.13) domi-
870 nating, Kmer_jump (0.11) secondary, and the remaining families contributing
871 negligibly. Random Forest integrates both Clipping (0.088) and Kmer_jump
872 (0.08) effectively, while SA_structure, Micro_homology, and Other remain minor
873 contributors. L₂-regularized Logistic Regression emphasizes Clipping (0.09)
874 and SA_structure (0.07), with Kmer_jump and Micro_homology having minimal
875 impact.

876 Both feature-level and aggregated analyses indicate that detection of chimeric
877 reads in this dataset relies primarily on alignment disruptions (Clipping) and
878 k-mer compositional shifts (Kmer_jump), which often arise from PCR-induced
879 recombination events, while explicit microhomology features contribute minimally.

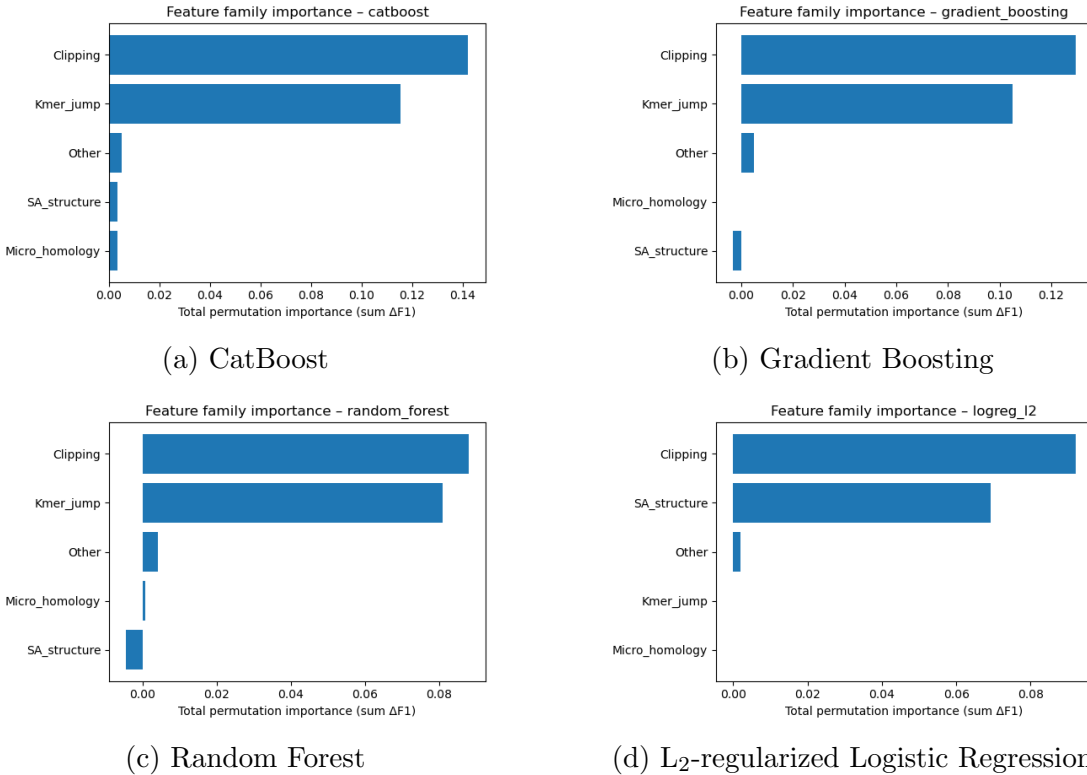


Figure 4.7: Aggregated feature family importance across four models. Clipping and k-mer compositional shifts are consistently the dominant contributors, while SA_structure, Micro_homology, and other features contribute minimally.

880 4.6 Summary of Findings

881 After removing trivially discriminative metadata, all models performed substan-
 882 tially better than the dummy baseline, with test F1-scores around 0.76 and ROC-
 883 AUC values near 0.84. Hyperparameter tuning yielded modest improvements,
 884 with boosting methods, particularly CatBoost and gradient boosting, achieving
 885 the highest performance. Confusion matrices and precision-recall curves indicate
 886 that these models prioritise precision for chimeric reads while accepting lower re-
 887 call, which a conservative strategy appropriate for scenarios where false positives

888 are costly.

889 Feature importance analyses revealed that alignment disruptions, such as clip-
890 ping, and abrupt k-mer composition changes accounted for most predictive power.
891 In contrast, microhomology metrics and supplementary alignment descriptors con-
892 tributed minimally. These results indicate that features based on read alignment
893 and k-mer composition are sufficient to train classifiers for detecting mitochon-
894 drial PCR-induced chimera reads, without needing additional quality-score or
895 positional information in the conditions tested.

⁸⁹⁶ References

- ⁸⁹⁷ Anderson, S., Bankier, A., Barrell, B., Bruijn, M., Coulson, A., Drouin, J., ...
⁸⁹⁸ Young, I. (1981, 04). Sequence and organization of the human mitochondrial
⁸⁹⁹ genome. *Nature*, *290*, 457-465. doi: 10.1038/290457a0
- ⁹⁰⁰ Arango, G., Garner, E., Pruden, A., Heath, L., Vikesland, P., & Zhang, L. (2018,
⁹⁰¹ 02). Deeparg: A deep learning approach for predicting antibiotic resistance
⁹⁰² genes from metagenomic data. *Microbiome*, *6*. doi: 10.1186/s40168-018
⁹⁰³ -0401-z
- ⁹⁰⁴ Bentley, D. R., Balasubramanian, S., Swerdlow, H. P., Smith, G. P., Milton, J.,
⁹⁰⁵ Brown, C. G., ... Smith, A. J. (2008). Accurate whole human genome
⁹⁰⁶ sequencing using reversible terminator chemistry. *Nature*, *456*(7218), 53–
⁹⁰⁷ 59. doi: 10.1038/nature07517
- ⁹⁰⁸ Boore, J. L. (1999). Animal mitochondrial genomes. *Nucleic Acids Research*,
⁹⁰⁹ *27*(8), 1767–1780. doi: 10.1093/nar/27.8.1767
- ⁹¹⁰ Cameron, S. L. (2014). Insect mitochondrial genomics: Implications for evolution
⁹¹¹ and phylogeny. *Annual Review of Entomology*, *59*, 95–117. doi: 10.1146/
⁹¹² annurev-ento-011613-162007
- ⁹¹³ Dierckxsens, N., Mardulyn, P., & Smits, G. (2017). Novoplasty: de novo assembly
⁹¹⁴ of organelle genomes from whole genome data. *Nucleic Acids Research*,

- 915 45(4), e18. doi: 10.1093/nar/gkw955
- 916 Edgar, R. C. (2016). Uchime2: improved chimera prediction for amplicon se-
917 quencing. *bioRxiv*. Retrieved from <https://api.semanticscholar.org/>
918 CorpusID:88955007
- 919 Edgar, R. C. (n.d.). *Uchime in practice*. Retrieved from https://www.drive5.com/usearch/manual7/uchime_practical.html
- 920 Edgar, R. C., Haas, B. J., Clemente, J. C., Quince, C., & Knight, R. (2011).
921 Uchime improves sensitivity and speed of chimera detection. *Bioinformatics*,
922 27(16), 2194–2200. doi: 10.1093/bioinformatics/btr381
- 923 Glenn, T. C. (2011). Field guide to next-generation dna sequencers. *Molecular
924 Ecology Resources*, 11(5), 759–769. doi: 10.1111/j.1755-0998.2011.03024.x
- 925 Gonzalez, J. M., Zimmermann, J., & Saiz-Jimenez, C. (2004, 09). Evalu-
926 ating putative chimeric sequences from pcr-amplified products. *Bioin-
927 formatics*, 21(3), 333-337. Retrieved from <https://doi.org/10.1093/bioinformatics/bti008>
928 doi: 10.1093/bioinformatics/bti008
- 929 Gray, M. W. (2012). Mitochondrial evolution. *Cold Spring Harbor perspectives
930 in biology*, 4. Retrieved from <https://doi.org/10.1101/cshperspect.a011403>
931 doi: 10.1101/cshperspect.a011403
- 932 Hahn, C., Bachmann, L., & Chevreux, B. (2013). Reconstructing mitochondrial
933 genomes directly from genomic next-generation sequencing reads—a baiting
934 and iterative mapping approach. *Nucleic Acids Research*, 41(13), e129. doi:
935 10.1093/nar/gkt371
- 936 Jin, J.-J., Yu, W.-B., Yang, J., Song, Y., dePamphilis, C. W., Yi, T.-S., & Li,
937 D.-Z. (2020). Getorganelle: a fast and versatile toolkit for accurate de
938 novo assembly of organelle genomes. *Genome Biology*, 21(1), 241. doi:
939 10.1186/s13059-020-02154-5
- 940

- 941 Judo, M. S. B., Wedel, W. R., & Wilson, B. H. (1998). Stimulation and sup-
942 pression of pcr-mediated recombination. *Nucleic Acids Research*, *26*(7),
943 1819–1825. doi: 10.1093/nar/26.7.1819
- 944 Labrador, K., Agmata, A., Palermo, J. D., Ravago-Gotanco, R., & Pante, M. J.
945 (2021). Mitochondrial dna reveals genetically structured haplogroups of
946 bali sardinella (sardinella lemuru) in philippine waters. *Regional Studies in*
947 *Marine Science*, *41*, 101588. doi: 10.1016/j.rsma.2020.101588
- 948 Layer, R., Hall, I., & Quinlan, A. (2014, 10). Lumpy: A probabilistic framework
949 for structural variant discovery. *Genome Biology*, *15*. doi: 10.1186/gb-2014
950 -15-6-r84
- 951 Li, H. (2018, 05). Minimap2: pairwise alignment for nucleotide sequences. *Bioin-*
952 *formatics*, *34*(18), 3094-3100. Retrieved from <https://doi.org/10.1093/bioinformatics/bty191>
953 doi: 10.1093/bioinformatics/bty191
- 954 Liang, Q., Bible, P. W., Liu, Y., Zou, B., & Wei, L. (2020, 02). Deepmi-
955 crobes: taxonomic classification for metagenomics with deep learning. *NAR*
956 *Genomics and Bioinformatics*, *2*(1), lqaa009. Retrieved from <https://doi.org/10.1093/nargab/lqaa009>
957 doi: 10.1093/nargab/lqaa009
- 958 Metzker, M. L. (2010). Sequencing technologies — the next generation. *Nature*
959 *Reviews Genetics*, *11*(1), 31–46. doi: 10.1038/nrg2626
- 960 Mysara, M., Saeys, Y., Leys, N., Raes, J., & Monsieurs, P. (2015). Catch,
961 an ensemble classifier for chimera detection in 16s rrna sequencing stud-
962 ies. *Applied and Environmental Microbiology*, *81*(5), 1573-1584. Retrieved
963 from <https://journals.asm.org/doi/abs/10.1128/aem.02896-14> doi:
964 10.1128/AEM.02896-14
- 965 Peccoud, J., Lequime, S., Moltini-Conclois, I., Giraud, I., Lambrechts, L., &
966 Gilbert, C. (2018, 04). A survey of virus recombination uncovers canon-

- 967 ical features of artificial chimeras generated during deep sequencing li-
968 brary preparation. *G3 Genes—Genomes—Genetics*, 8(4), 1129-1138. Re-
969 trieved from <https://doi.org/10.1534/g3.117.300468> doi: 10.1534/
970 g3.117.300468
- 971 Qin, Y., Wu, L., Zhang, Q., Wen, C., Nostrand, J. D. V., Ning, D., ... Zhou, J.
972 (2023). Effects of error, chimera, bias, and gc content on the accuracy of
973 amplicon sequencing. *mSystems*, 8(6), e01025-23. Retrieved from <https://journals.asm.org/doi/abs/10.1128/msystems.01025-23> doi: 10.1128/
974 msystems.01025-23
- 975 Qiu, X., Wu, L., Huang, H., McDonel, P. E., Palumbo, A. V., Tiedje, J. M., &
976 Zhou, J. (2001). Evaluation of pcr-generated chimeras, mutations, and het-
977 eroduplexes with 16s rrna gene-based cloning. *Applied and Environmental
978 Microbiology*, 67(2), 880–887. doi: 10.1128/AEM.67.2.880-887.2001
- 980 Ren, J., Song, K., Deng, C., Ahlgren, N., Fuhrman, J., Li, Y., ... Sun, F. (2020,
981 01). Identifying viruses from metagenomic data using deep learning. *Quan-
982 titative Biology*, 8. doi: 10.1007/s40484-019-0187-4
- 983 Rodriguez-Martin, B., Palumbo, E., Marco-Sola, S., Griebel, T., Ribeca, P.,
984 Alonso, G., ... Djebali, S. (2017, 01). Chimpipe: Accurate detection of
985 fusion genes and transcription-induced chimeras from rna-seq data. *BMC
986 Genomics*, 18. doi: 10.1186/s12864-016-3404-9
- 987 Rognes, T., Flouri, T., Nichols, B., Quince, C., & Mahé, F. (2016). Vsearch: a
988 versatile open source tool for metagenomics. *PeerJ*, 4, e2584. doi: 10.7717/
989 peerj.2584
- 990 Sedlazeck, F., Rescheneder, P., Smolka, M., Fang, H., Nattestad, M., von Haeseler,
991 A., & Schatz, M. (2018, 06). Accurate detection of complex structural
992 variations using single-molecule sequencing. *Nature Methods*, 15. doi: 10

- 993 .1038/s41592-018-0001-7
- 994 995 996 997 998 Sfeir, A., & Symington, L. S. (2015). Microhomology-mediated end joining: A back-up survival mechanism or dedicated pathway? *Trends in Biochemical Sciences*, 40(11), 701-714. Retrieved from <https://www.sciencedirect.com/science/article/pii/S0968000415001589> doi: <https://doi.org/10.1016/j.tibs.2015.08.006>
- 999 1000 1001 1002 Vervier, K., Mahé, P., Tournoud, M., Veyrieras, J.-B., & Vert, J.-P. (2015, 11). Large-scale machine learning for metagenomics sequence classification. *Bioinformatics*, 32(7), 1023-1032. Retrieved from <https://doi.org/10.1093/bioinformatics/btv683> doi: 10.1093/bioinformatics/btv683
- 1003 1004 1005 1006 Willette, D., Bognot, E., Mutia, M. T., & Santos, M. (2011). *Biology and ecology of sardines in the philippines: A review* (Vol. 13; Tech. Rep. No. 1). NFRDI Technical Paper Series. Retrieved from <https://nfrdi.da.gov.ph/tpjf/etc/Willette%20et%20al.%20Sardines%20Review.pdf>